Environ. Sci. Technol. **1999**, *33,* 4046−4053

Partitioning Tracer Method for the In Situ Measurement of DNAPL Saturation: Influence of Heterogeneity and Sampling Method

NICOLE T. NELSON,[†,‡] MART OOSTROM,[§] TOM W. WIETSMA,[∥] AND MARK L. BRUSSEAU*[,†,⊥]

Department of Soil, Water, and Environmental Science and Department of Hydrology and Water Resources, Shantz Building, Room 429, University of Arizona, Tucson, Arizona 85721, and Environmental Technology Division and Environmental Molecular Science Laboratory, Pacific Northwest National Laboratory, Richland, WA 99352

The purpose of this work was to examine the effect of porous-media heterogeneity, nonuniform distribution of dense nonaqueous phase liquid (DNAPL), and sampling method on the performance of the partitioning tracer method for measuring DNAPL saturation in water-saturated subsurface systems. Experiments were conducted in an intermediate-scale flow cell that contained two discrete zones of trichloroethene (TCE) at residual saturation. One zone (zone 2) consisted of ∼10% saturation formed in the same sand as used for the flow-cell matrix. The other zone (zone 1) consisted of ∼10% saturation in a finer sand emplaced within the coarser matrix. Aqueous samples were collected using depth-specific sampling, using vertically integrated sampling, and at the extraction well. A dual-energy γ radiation system was used to measure TCE saturation before and after the tracer experiment, allowing the measurements obtained from the tracer experiment to be compared to a previously tested method. The saturations estimated using the data collected at point-sampling ports located downgradient of zones 1 and 2 were approximately 7% and 50% of the true values, respectively. The saturations estimated using the data obtained from the vertically integrated ports were 0% and 6% of the true values, respectively. Finally, the saturation estimated using the extraction-well data was 30% of the cell-wide averaged value. These results indicate that the presence of porous-media heterogeneity and a variable distribution of DNAPL saturation can lead to reduced accuracy of the partitioning tracer test. The reduced performance can be improved, in part, by using depth-specific sampling.

Introduction

Nonaqueous phase organic liquids (NAPLs) occur in the subsurface at numerous contaminated sites and can act as long-term sources of both vapor-phase and groundwater contamination. The presence of NAPL is often considered the single most important factor limiting the cleanup of sites contaminated by organic compounds (*1*). In fact, restoring groundwater to health-based goals using existing technologies (e.g., pump-and-treat) is considered infeasible at most sites contaminated by denser than water nonaqueous phase organic liquids (DNAPL). Thus, knowledge of the occurrence, quantity, and distribution of NAPL in the subsurface is critical for the planning and implementation of successful remediation strategies for NAPL-contaminated sites. Additionally, such knowledge can improve risk assessments of NAPL-contaminated sites.

Current methods used for characterizing sites potentially contaminated with a NAPL phase include analysis of soil gas, core sampling, cone penetrometer testing, and monitoring-well sampling (*2, 3*). These methods sample relatively small volumes of the subsurface and, therefore, require what is often a cost-prohibitive amount of sampling to accurately determine NAPL distribution. The partitioning tracer test is an alternative, larger-scale method for locating and quantifying NAPL saturation in the subsurface (*4*−*6*).

The partitioning tracer test is based on conducting a tracer test in the targeted zone of the subsurface. The potential presence of NAPL is evaluated by comparing the transport of one or more partitioning tracers to that of a nonreactive (nonpartitioning, nonsorbing) tracer. Organic fluid phases reversibly retain the partitioning tracer, which retards its transport with respect to that of a nonreactive tracer. For a given partitioning tracer, the magnitude of retardation is correlated to the amount of NAPL encountered. The partitioning tracer test was introduced in the petroleum engineering field as a means to measure residual oil (*7*−*9*). It has recently been used at several hazardous waste sites to detect and quantify NAPL saturation (*6, 10*−*14*).

There are several factors that can constrain the performance of partitioning tracer tests. These factors include the presence of subsurface heterogeneity, variable distribution of NAPL, rate-limited mass transfer, tracer mass loss, and sampling method. For example, groundwater may flow primarily around (bypass) zones of higher NAPL saturation due to the reduced aqueous relative permeabilities associated with these zones. This bypass flow may reduce the contact between the tracer solution and the NAPL, thereby resulting in an underestimate of NAPL saturation. Furthermore, NAPL trapped in lower permeability zones may be difficult to measure with the partitioning tracer test due to preferential flow associated with the porous-media heterogeneity. The influence of these factors on the efficacy of the partitioning tracer method has not been investigated in detail.

The purpose of this work is to examine the effect of three of these factors (porous-media heterogeneity, variable NAPL distribution, and sampling method) on the performance of the partitioning tracer method. Miscible displacement experiments were conducted using an intermediate-scale flow cell packed with a homogeneous sand in which were placed two zones of residual TCE saturation. One was created in the same sand as the matrix and the other was created in a finer sand. Aqueous samples were collected using depth-specific sampling, using vertically integrated sampling, and at the extraction well.

Materials and Methods

Experimental Apparatus. The experiments were conducted in a 2.20 m long by 1.1 m high by 0.053 m wide flow cell (Figure 1). The flow cell was constructed with a 0.64 cm thick

* Corresponding author e-mail: brusseau@ag.arizona.edu; phone: (520)621-3244; fax: (520)621-1647.

[†] Department of Hydrology and Water Resources.

[‡] Present address: Daniel B. Stephens & Associates, Inc., Albuquerque, NM.

[§] Environmental Technology Division.

[∥] Environmental Molecular Science Laboratory.

[⊥] Department of Soil, Water, and Environmental Science.

10.1021/es990022p CCC: $18.00 © 1999 American Chemical Society
Published on Web 10/07/1999

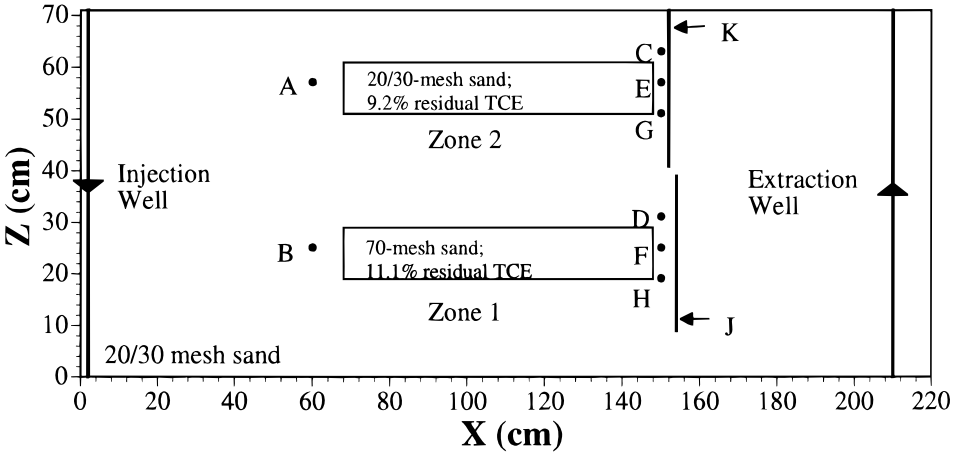

FIGURE 1. Schematic of flow cell.

glass front plate to allow flow visualization and a 0.64 cm thick Kynar back plate to allow for installation of sampling ports. The glass and Kynar plates were attached to a 2.54 cm thick stainless steel frame. Vertical 3.18 cm rectangular bars, spaced approximately 22 cm apart and welded to 2.54 cm angle iron at the top and bottom, provided support for the cell.

The flow cell was equipped with eight "point" sampling ports (Figure 1, A−H), which were integrated across the 0.053 m width, and two "vertically integrated" sampling ports ports (Figure 1, J and K), which were integrated across the 0.053 m width and a 0.3 m height. The point-sampling ports were designed to emulate multilevel samplers, whereas the vertically integrated sampling ports were designed to emulate monitoring wells with relatively large screened intervals. The point-sampling ports consisted of laser-drilled stainless steel tubing (0.18 cm o.d. and 4.8 cm length) that are inserted through holes drilled into the Kynar back and terminate in PEEK push valves (Kloehn, Las Vegas). The vertically integrated sampling consisted of three lengths of the same type of stainless steel tubing inserted through the top of the flow cell at the same *X* coordinate (length) but spaced evenly along the *Z* coordinate (width). The three tubes were connected via a manifold that terminated in a PEEK push valve.

An injection well and an extraction well, each consisting of 2.2 cm i.d. Schedule 40 PVC pipe slotted over a 71 cm length, were installed at opposite ends of the flow cell. To reduce dead volume, solid aluminum rods with 1.6 cm o.d. were placed within the PVC. A zone of pea gravel was packed around the PVC wells to ensure uniform tracer injection. A cotton cloth sleeve was wrapped around the slots to reduce clogging.

Materials. Calcium bromide (bromide) and 2,4-dimethyl-3-pentanol (DMP) served as the nonreactive and partitioning tracers, respectively. Trichloroethene (TCE) was used as the representative DNAPL. The TCE was dyed with a hydrophobic red dye, Sudan IV (0.1 g/L), to allow visualization of the TCE phase. Fluorescein dye (sodium salt form) was used to conduct visualization experiments to help characterize the flow field. Research grade bromide, TCE, and the fluorescein dye (∼70% dye content) were purchased from Aldrich Chemical Co., Inc., Milwaukee, WI. Research-grade DMP was purchased from Lancaster Chemicals. The partitioning tracer was chosen based on preliminary batch experiments conducted to measure the TCE−water partition coefficient, which is 46.5.

The porous media used in this study were a medium-grained (20/30 mesh) sand used for the matrix and a fine-grained (70 mesh) sand used to create a lower permeability inclusion (Unimin Corporation, Le Sueur, MN). Information on the particle diameters, uniformity coefficients, particle densities, and permeabilities of the sands is listed in Table 1. The TCE entry pressures of the 20/30- and 70-mesh sands, determined using the pressure cell method described by Lenhard (*17*), are 420 and 2180 Pa, respectively. These correspond to TCE pressure heads of approximately 4.2 and 21.8 cm, respectively.

TABLE 1. Physical Properties of the 20/30- and 70-Mesh Sands

	70-mesh	20/30-mesh
particle diameter, d_{50}[a] (mm)	0.213 ± 0.001	0.724 ± 0.031
uniformity coefficient d_{60}/d_{10}[b]	1.210 ± 0.034	1.184 ± 0.039
particle density (kg/m^3)	2658	2657
permeability (m^2)	2.6E−12	1.38E−10

[a] Five sieve analyses were performed for each sand using methods described in ref *15*. [b] Determined using method described in ref *16*.

TABLE 2. Average Properties of the Two TCE Residual Saturation Zones

	zone 1	zone 2
Computed Gravimetrically and Volumetrically		
dry bulk density (kg/m^3)	1637	1759
porosity	0.384	0.338
TCE saturation	0.122	0.116
Computed from γ Data		
path length, cm	5.29 ± 0.08	5.28 ± 0.07
dry bulk density (kg/m^3)	1659	1764
porosity	0.376 ± 0.012	0.336 ± 0.017
initial TCE saturation	0.111 ± 0.010	0.092 ± 0.011
final TCE saturation	0.101 ± 0.030	0.062 ± 0.039
relative permeability	0.71	0.75
effective permeability (m^2)	1.85E−12	1.04E−10

Experimental Procedures. Two distinct zones containing residual TCE were established in the flow cell (Figure 1). Zone 1 contained residual TCE within 70-mesh sand to examine the effect of preferential flow associated with physical heterogeneity on tracer transport. This zone represents a system wherein site conditions may promote penetration of immiscible liquid into lower permeability layers (in this case a fine sand). This situation can occur at sites where the disposal practices allowed the development of a vertically contiguous DNAPL zone. In such cases, it is likely that isolated zones of residual saturation will reside in the finer-grained media, given that residual DNAPL will dissolve more quickly from the more conductive zones. Zone 2 contained residual TCE within the same sand as comprised the matrix and is used to examine the effect of bypass flow

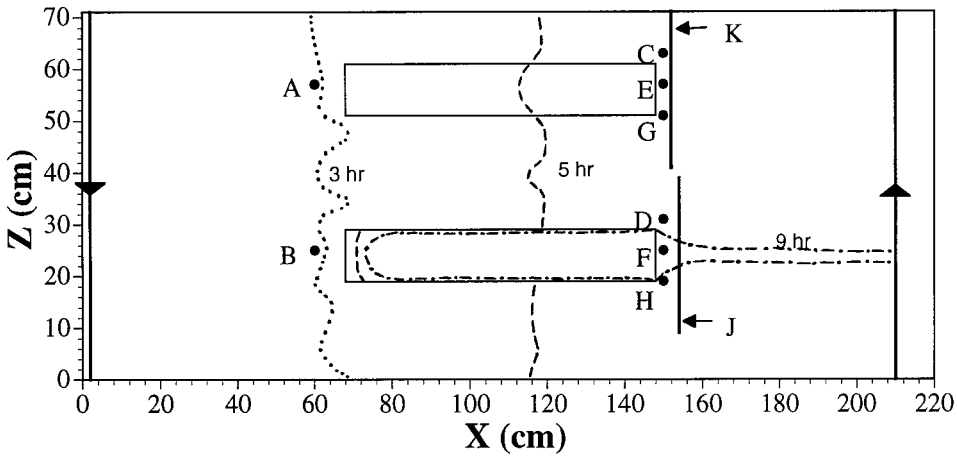

FIGURE 2. Schematic drawing of dye experiment results.

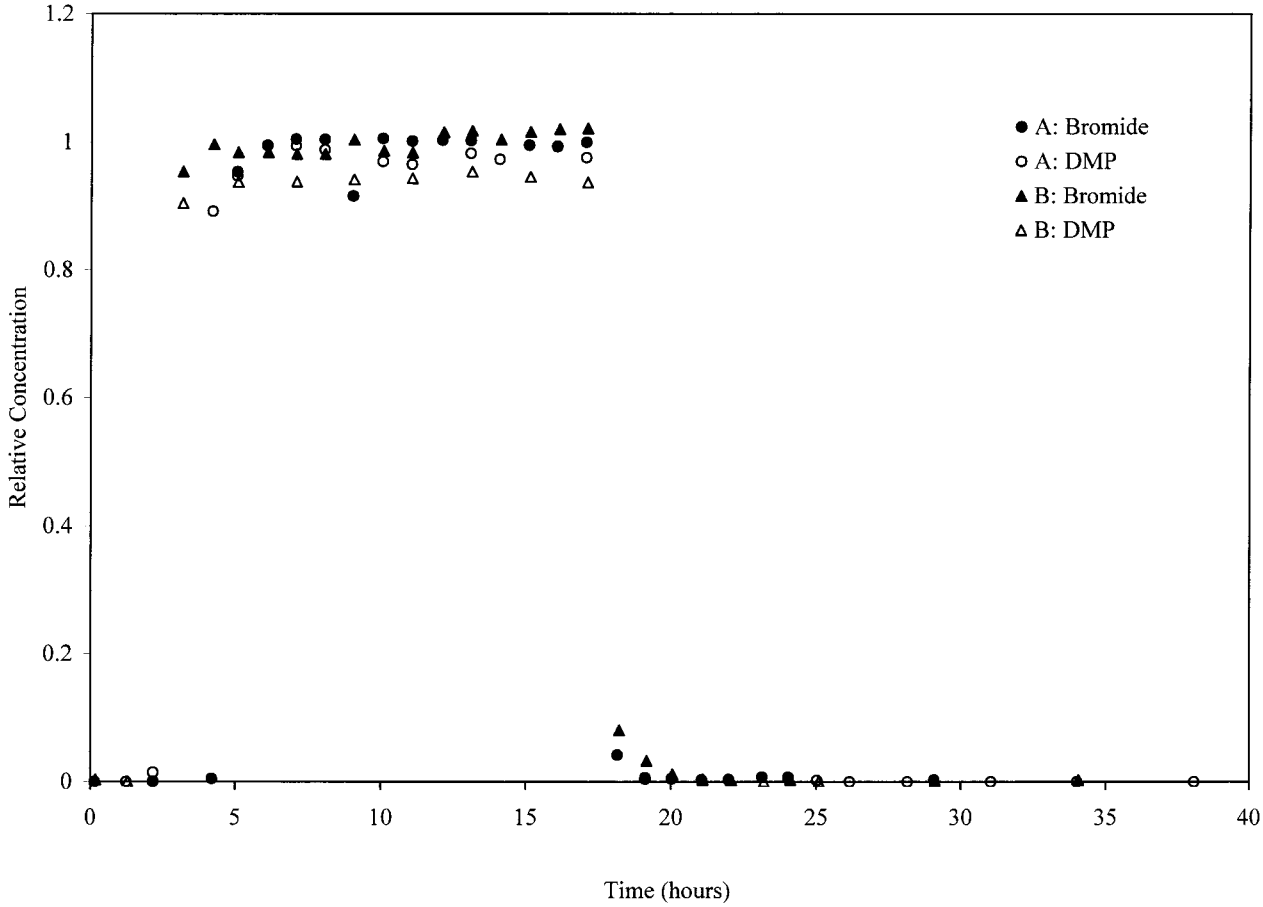

FIGURE 3. Tracer breakthrough curves measured at point-sampling ports (A and B) located upgradient of the TCE residual saturation zones.

associated with the reduced relative permeability caused by a localized zone of TCE saturation.

The two TCE residual zones (0.8 m long by 0.1 m high by 0.053 m wide blocks) were emplaced in the flow cell as follows. First, the flow cell was packed under water-saturated conditions with 20/30-mesh sand to a height coincident with the lower boundary of each of the planned inclusions. The water table was then lowered until the upper 1 cm of the 20/30-mesh sand had drained. The TCE residual zones were then emplaced within the designated locations, using vertical slats for temporary support. For each zone, the sand/TCE mixture was prepared by thoroughly mixing a predetermined amount of damp sand (volumetric moisture content of ~10%) with an amount of liquid TCE that would yield an approximate 10% saturation of the pore space. After flushing each emplaced zone with CO_2 to assist saturation by water, the water level was slowly raised. After packing was completed (total sand-pack height was 0.7 m), a 1-cm-layer of a kaolinite-clay paste was placed on top of the sand to create an impermeable cap. On the basis of the amount of sand and liquid TCE packed in each zone, average bulk densities, porosities, and TCE saturations were computed for the two zones (Table 2).

After the flow cell was packed and an initial set of dual-energy γ radiation measurements were collected, steady-state flow was established by flushing a 750 mg/L solution of $CaCl_2$ through the flow cell using two Masterflex peristaltic pumps. The injection and extraction flow rates were gradually increased to and remained at 50 ± 0.7 mL/min. Once steady-state conditions were achieved, a pulse of tracer solution

TABLE 3. Moment Analysis Results

	bromide		DMP				
	zeroth moment (h)	travel time (h)	zeroth moment (h)	travel time (h)	R	S_n (estd)[a] (%)	S_n (measd)[b] %)
port A	14.0	3.7	14.5	3.2	0.87		
port B	16.1	2.4	15.0	2.75	1.10		
port C	14.2	7.1	11.4	6.4	0.89		
port D	15.4	7.2	14.1	7.1	0.99		
port E	15.4	7.8	13.9	18.1	2.31	1.9	4.6
port F	14.7	13.1	13.1	17.0	1.30	0.4	5.9
port G	15.4	8.4	14.7	24.7	3.05	2.9	4.6
port H	16.2	12.7	16.2	13.4	1.29	0.4	5.9
port J	15.3	7.3	14.5	7.0	0.96	0	2.0
port K	14.2	7.4	12.1	7.7	1.04	0.09	1.5
EXT	15.1	14.8	14.1	17.6	1.18	0.3	1.0

[a] Values estimated from tracer data. [b] Values measured using the dual-energy γ system (values are averaged over appropriate space and time domains).

containing 170 mg/L bromide and 180 mg/L DMP was injected for 15 h. The tracer solution also contained $CaCl_2$ to match the density of the electrolyte solution. Following the tracer pulse, tracer-free water was flushed through the system for 130 h.

The point and vertically integrated ports were sampled by attaching a gas-tight 10-mL syringe with a glass barrel (Kloehn, Las Vegas or Hamilton) to the push valve connected to a particular port. A 1-mL purge volume was discarded prior to taking a sample. Following the purge, a 6-mL sample was withdrawn. Two milliliters was used to completely fill glass vials with Teflon-lined septums for analysis of DMP and TCE. Four milliliters was expelled into polyethylene vials for analysis of bromide. The extraction-well effluent was sampled by allowing free flow into the vials. The samples were stored at 5 °C prior to analysis.

A transport experiment using a fluorescent dye (fluorescein) was conducted to qualitatively examine the uniformity of packing and the effect of the heterogeneities on the flow field. The experiment was conducted after the tracer test to avoid potential interaction of the dye with the porous-media or NAPL phase. Steady-state flow was maintained between the tracer test and the dye experiment. The experiment was implemented by injecting a pulse of water containing 200 mg/L fluorescein through the flow cell at 50 mL/min, followed by continuous injection of dye-free water. Photographs were periodically taken during the experiment.

Dual-Energy γ Radiation Measurements. The flow cell was designed to be compatible with a fully automated dual-energy (280 mCi of americium and 100 mCi of cesium) γ radiation system, which was used to determine TCE saturations in the two zones. Each zone was calibrated at 792 measurement locations according to procedures adapted from Oostrom and colleagues (*18, 19*). The horizontal and vertical distance between measurement locations was 1 cm except where vertical support bars were present. The horizontal distance between locations at either side of a vertical support bar was 5 cm. In the calibration procedure, count rates were obtained at all locations when the flow cell was empty and filled with water for path length determinations. To obtain TCE saturations, the flow cell was scanned prior to injection of the tracer solution into the flow cell, after injection/extraction was terminated, and after remediation of both zones with a 4% anionic surfactant solution. Because the TCE was added to the flow cell concurrent with packing, it was necessary to remove all TCE from the two zones after the tracer experiment to obtain γ counts without liquid TCE present (i.e., to establish background). The counting times for all scans were 60 s per location.

Analytical Methods and Data Analysis. The DMP and TCE were analyzed using a Shimadzu gas chromatograph with flame ionization detector (model 14A) equipped with a Shimadzu auto injector (model AOC-17). The detection limit of DMP and TCE were 1.4 and 0.3 mg/L, respectively. The bromide was analyzed using a Dionex ion chromatograph (model DX-500) with suppressed conductivity detector. The detection limit of bromide was 100 μg/L.

The procedure for estimating NAPL saturation, S_n, involves calculation of a retardation factor (R) for the partitioning tracer, which is done by a comparative moment analysis with the nonreactive tracer. The retardation factor is defined as the quotient of the travel times of the partitioning and nonreactive tracers. With knowledge of R and the NAPL–water partition coefficient (K_{nw}), S_n can be calculated, assuming no sorption, from (e.g., *4* and *20*):

$$R = 1 + [S_n/(1 - S_n)]K_{nw} \quad (1)$$

Results and Discussion

Dual-Energy γ Radiation Measurements. The path lengths, dry bulk densities, porosities, and TCE saturations obtained from the dual-energy γ measurements for the two TCE residual saturation zones at the start and end of the tracer experiment are reported in Table 2. The average values computed from the γ radiation data are similar to the values obtained gravimetrically. The smaller TCE saturations obtained with the γ data reflect the impact of TCE volatilization during packing, which is not incorporated in the gravimetric based calculations. The γ data were used to calculate an average porosity and bulk density of 0.331 cm^3/cm^3 and 1763 kg/m^3, respectively, for the flow-cell matrix.

Aqueous-phase relative permeabilites for both zones were calculated using relationships based on the Mualem pore-size distribution model (*21*), as discussed by Lenhard and Parker (*22*). A primary assumption associated with the calculations is that the entrapped TCE is uniformly distributed over the entire pore space. Considering that the TCE was mixed with the sand initially, this is a viable assumption in our case. The effective permeabilities reported in Table 2 were computed as the product of the relative permeability of each zone and the permeability of the corresponding "TCE-free" sand.

Tracer Transport. *Nonreactive Tracer and Dye Transport.* The dye pulse was characterized by a relatively sharp vertical front as it traveled through the region upgradient of the heterogeneities, indicating fairly uniform packing (Figure 2, 3 h). However, the behavior of the pulse indicated nonuniform flow behavior associated with zones 1 and 2. The dye was delayed slightly by zone 2 and significantly by zone 1 (Figure 2, 5 h), as expected based on their respective permeabilites. Dye-free regions persisted downgradient of both zones, especially zone 1, indicating areas of no flow (Figure 2, 9 h).

Breakthrough curves measured for bromide and DMP at the two point-sampling ports (A and B) located upgradient from the TCE zones are shown in Figure 3. The breakthrough curves are sharp and symmetrical, indicating that packing was uniform. This is consistent with the results of the dye experiment. The positions and general shapes of the DMP breakthrough curves are very similar to those of bromide at these locations. This indicates that DMP experienced no measurable sorption by the solid phase and also that its dispersive flux was similar to that of bromide. The data for the tracers were analyzed by calculating the zeroth and first temporal moments to quantify mass recovery and retardation, which are presented in Table 3. The difference in travel times calculated for ports A and B is primarily due to insufficient sampling of the sharp tracer fronts.

Point Sampling Ports (Zone 2). Breakthrough curves measured for bromide and DMP at a point-sampling port

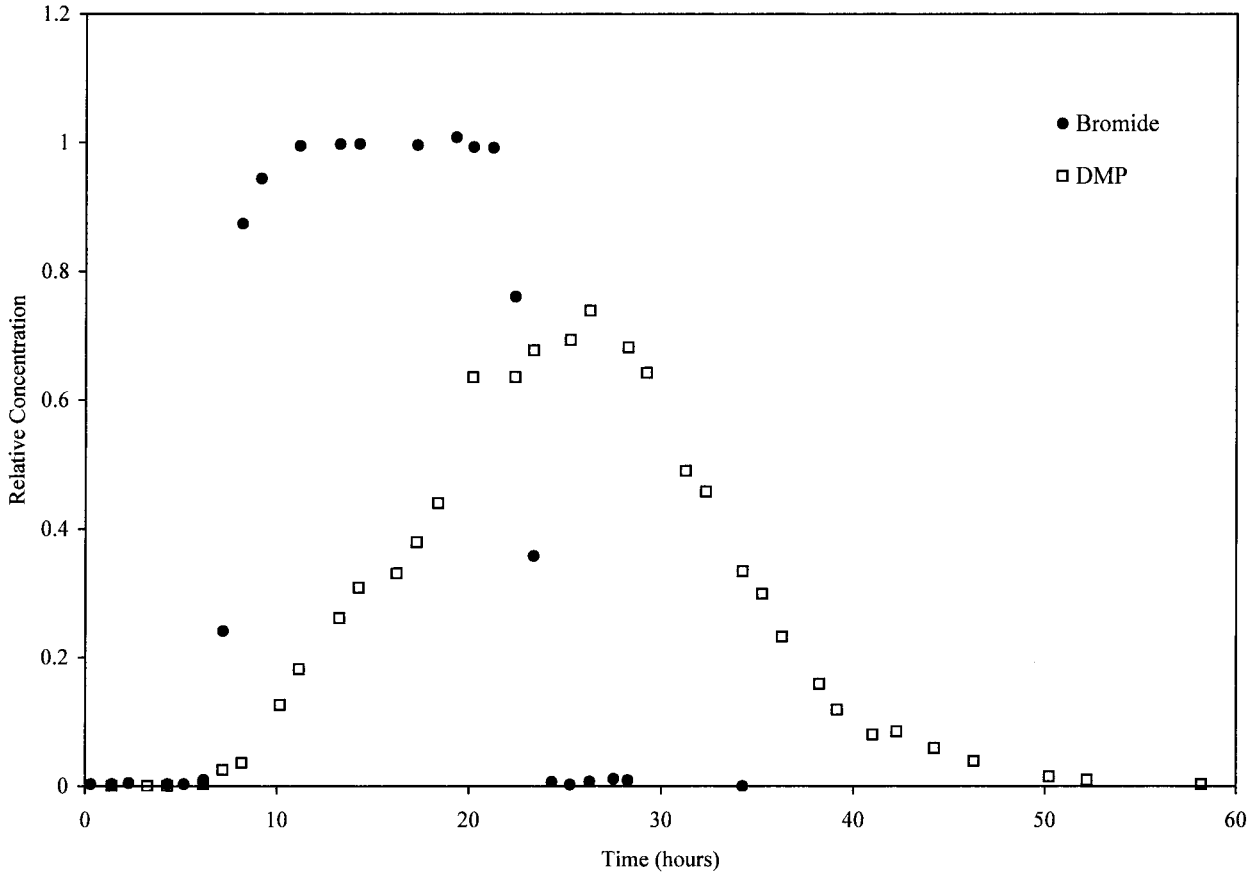

FIGURE 4. Tracer breakthrough curves measured at a point-sampling port (E) located downgradient of TCE residual saturation zone 2.

(E) located downgradient of zone 2 are shown in Figure 4. The arrival of the DMP breakthrough curve is clearly delayed in comparison to that of bromide. Similar behavior was observed for port G (data not shown), which is also downgradient of zone 2. However, no retardation was observed for the DMP breakthrough curve measured at port C (data not shown), which while also downgradient is approximately 3 cm above the top of zone 2.

Given that partitioning into the immiscible liquid phase of TCE is the only mechanism causing retention of DMP, apparent TCE saturations can be calculated using eq 1. The saturation values estimated using the data collected at ports E and G are 1.9% and 2.9%, respectively. It is critical to note that these saturations represent average values that are integrated across the entire tracer-swept region associated with the injection/sampling points.

The values determined with the partitioning tracer test can be compared to those obtained with the dual-energy γ measurements made prior to the tracer experiment. However, these values must be averaged over the tracer-swept region to allow direct comparison to the S_n values determined with the tracer test. Assuming horizontal flow and considering that the area upgradient of zone 2 did not contain TCE saturation, the spatially averaged value is calculated to be 5.0%. Additionally, the S_n estimated from the tracer data should be compared to a measured S_n value that is temporally averaged, given that the TCE saturation decreased during the experiment due to dissolution. For example, using the dual-energy γ system, a S_n value of 6.2% was measured for zone 2 at the end of the tracer test. This corresponds to a spatially averaged value of 3.3%. Thus, the spatially averaged S_n for zone 2 ranged between 5 and 3.3% during the course of the experiment. The total mass of TCE removed after 30 h (as determined by monitoring the elution curve) was used to specify a more precise temporally averaged S_n value. The 30-h time point was selected to be larger than all mean travel times. The total mass removed was apportioned between zones 1 and 2 by comparing the masses removed from the two zones according to the dual-energy γ data. This mass removal analysis yields a spatially and temporally averaged S_n value of 4.6% for the tracer-swept region associated with ports E and G.

Comparison of the S_n values obtained from analysis of the tracer test results to the independently measured value of 4.6% indicates that the partitioning tracer method measured 41% and 63% of the true values for ports E and G, respectively. Thus, the partitioning tracer method did not measure the total TCE saturation. This is primarily due to the preferential flow caused by the reduced permeability associated with the TCE saturation residing in zone 2. The higher S_n value measured for port G as compared to port E may be due in part to slightly higher S_n values at the bottom of the zone, as measured by the dual-energy γ system. Hydraulic factors, such as the presence of a possible lower-flow region in the vicinity of port E, as suggested by the results of the fluorescein dye experiment, may also contribute to the lower value obtained for port E.

Point Sampling Ports (Zone 1). Breakthrough curves measured for bromide and DMP at a point-sampling port (F) located downgradient of zone 1 are shown in Figure 5. The bromide breakthrough curve is asymmetrical and contains multiple peaks in the tail region, indicating that a nonuniform flow field is significantly influencing tracer transport. Similar behavior was observed for port H (data not shown). The permeability ratios between zone 1 and the matrix and between zone 2 and the matrix are 75 and 1.3, respectively. Thus, the degree of flow nonuniformity associated with zone 1 would be expected to be greater than that associated with zone 2. This difference would account for the distinct differences in the shapes and travel times of the

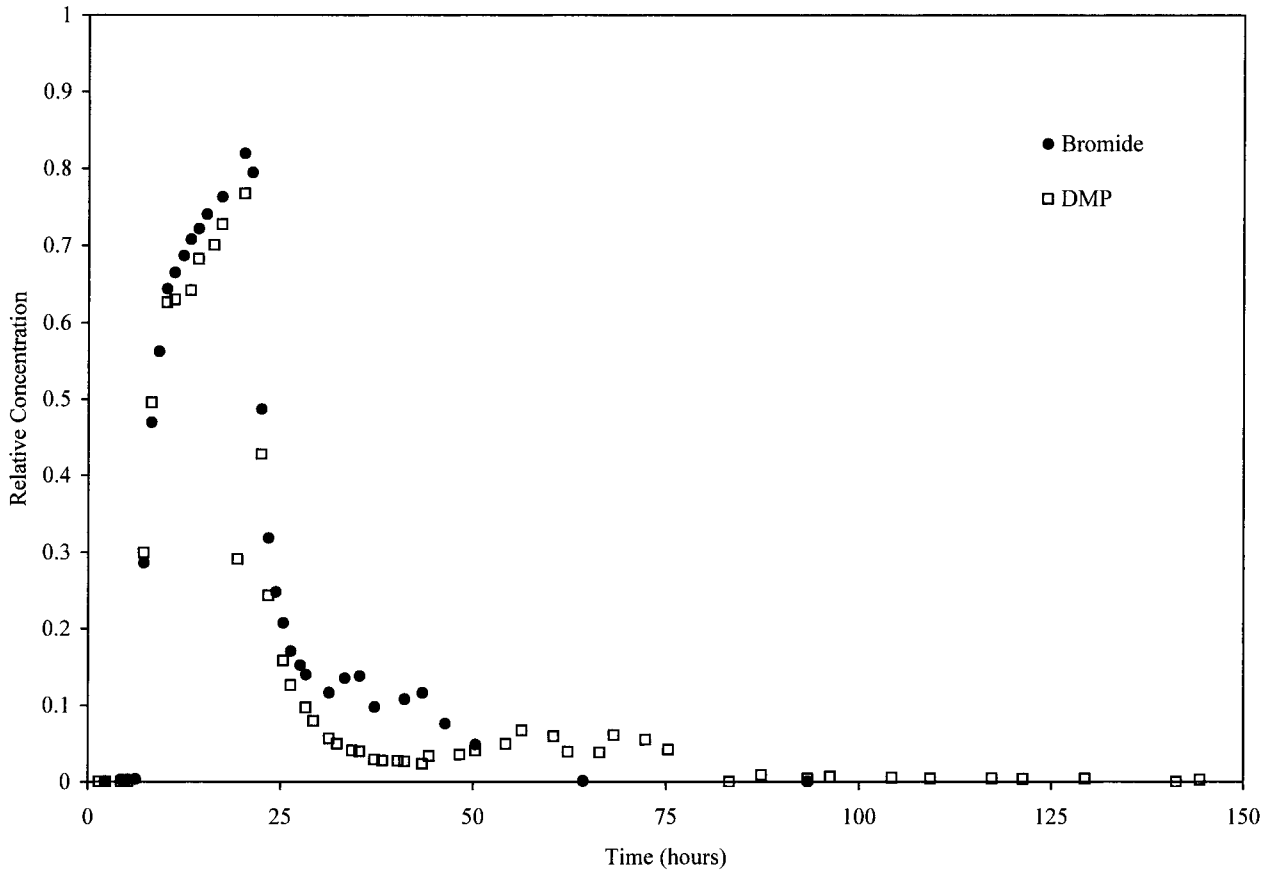

FIGURE 5. Tracer breakthrough curves measured at a point-sampling port (F) located downgradient of TCE residual saturation zone 1.

bromide breakthrough curves obtained at ports F and H as compared to those obtained at ports E and G. The difference in the degree of flow nonuniformity is supported by the results of the fluorescein dye experiment. Although the dye experiment highlighted regions of essentially no flow downgradient of both NAPL zones, the region downgradient of zone 1 was more persistent and had sharper boundaries.

The S_n values estimated using the data collected at the two ports (F and H) downgradient of zone 1 are both 0.4%. As described above, the S_n values measured with the dual-energy γ system need to be spatially and temporally averaged before they can be compared to the tracer results. Following the approach described above, the spatially and temporally averaged value for the tracer-swept region associated with ports F and H is estimated to be 5.9%. The S_n values measured by the partitioning tracer test are thus approximately 7% of the true value.

The lower values of S_n determined from the tracer data collected at ports F and H as compared to ports E and G indicate that the tracer method was less effective at measuring the NAPL retained within the lower intrinsic permeability zone. This reduced performance is due to the larger degree of preferential flow and related physical nonequilibrium associated with zone 1 relative to zone 2. As discussed above, the larger degree of nonuniform flow is supported by the asymmetrical breakthrough curves and the results of the dye experiment. Given this, the transport of the partitioning tracer in to and out of zone 1 is most likely controlled by diffusive mass transfer.

Vertically Integrated Ports and Extraction Well. Breakthrough curves measured for bromide and DMP at the vertically integrated ports located downgradient from zone 2 (port K) and zone 1 (port J) are shown in Figure 6. The position and general shape of the DMP breakthrough curves are very similar to those of bromide. The breakthrough curves

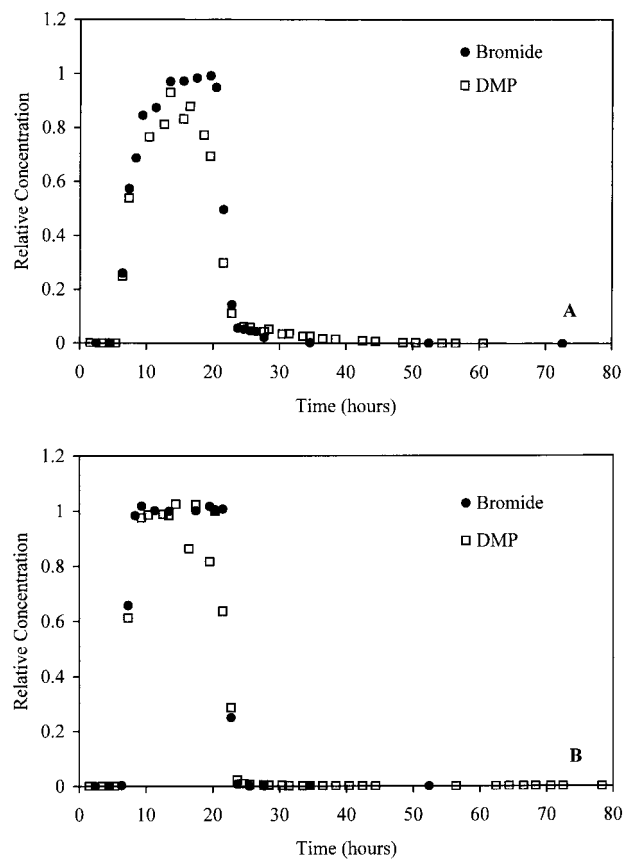

FIGURE 6. Tracer breakthrough curves measured at the vertically integrated sampling ports: (A) port K, downgradient of zone 2, (B) port J, downgradient of zone 1.

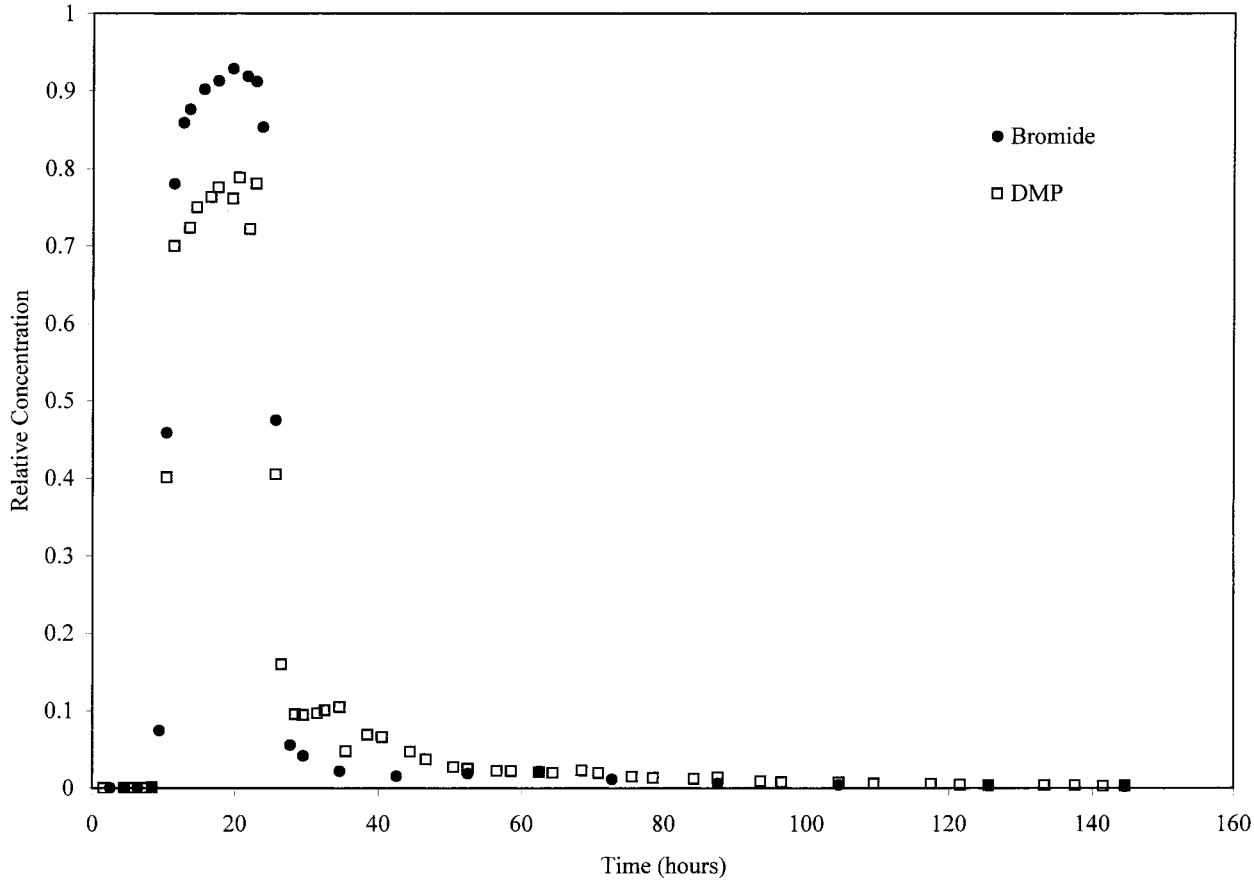

FIGURE 7. Tracer breakthrough curves measured at the extraction well.

for port J are sharper than those obtained for port K, most likely due to the fact that the difference in permeability between zone 1 and the surrounding matrix is such that most of the water entering the vertically integrated port comes from the surrounding coarser matrix. The moment analysis yields retardation factors of 1.04 (port K) and 1 (port J) for DMP, which correspond to S_n values of 0.09% and 0%, respectively. These values severely underestimate the true spatially and temporally averaged S_n values, which are 1.5% and 2.0% for the tracer-swept regions associated with ports K and J, respectively.

Breakthrough curves measured for bromide and DMP at the extraction well are shown in Figure 7. Although the fronts arrive at the same time, DMP exhibits more tailing than bromide. The S_n calculated using eq 1 is 0.3%. The swept volume for the extraction well consists of the entire flow cell. Therefore, the S_n values obtained from the dual-energy γ data must be averaged over the entire flow cell. This spatially averaged S_n is 1.1% before the tracer experiment and 0.9% at the end of the tracer experiment, which translates to a temporally averaged S_n of 1.0%. Thus, the partitioning tracer data collected at the extraction well yields a value that is 30% of the true value.

Summary. The results of these experiments demonstrate that preferential flow and physical nonequilibrium associated with zones of lower intrinsic and relative permeability can have a significant impact on the performance of the partitioning tracer test. The results also show that this impact varies as a function of the sampling method. The highest S_n estimates were obtained from data collected at the point-sampling ports. The lowest values of NAPL saturation were obtained from the data collected at the vertically integrated sampling ports. These results illustrate the inherent difficulty in using vertically integrated sampling to accurately characterize heterogeneous systems. The comparatively large vertical sampling intervals associated with the vertically integrated ports intercept a large fraction of streamlines that have not contacted the NAPL phase. In addition, the samples, which are flux-averaged, are biased toward the zones of higher relative permeability (i.e., those with little or no NAPL saturation). Given these results, it appears that the use of depth-specific sampling should be considered for enhancing the performance potential of the partitioning tracer method, especially for heterogeneous systems.

Although the quantitative performance of the partitioning tracer test may in some cases be constrained by factors such as those investigated herein, the method is a viable tool for characterizing sites that may be contaminated by NAPL. At sites where the presence of NAPL is suspected but not confirmed, partitioning tracers may be useful as "detectors" of NAPL saturation. Partitioning tracers may also be useful as "performance indicators" of a chosen remedial action. Tracer tests can be conducted before, during, and after site cleanup to evaluate the relative performance of the remediation system. Additional research in this area is certainly justified due to a continued need to characterize the large number of sites contaminated by complex and persistent NAPL phases.

Acknowledgments

This research was supported by a grant from the U.S. Department of Energy Environmental Management Science Program. Pacific Northwest National Laboratory is operated by the Battelle Memorial Institute for the U.S. DOE under Contract DE-AC06-76RLO 1830. Support provided by the PNNL Environmental Molecular Science Laboratory is gratefully acknowledged. We thank Gwynn Johnson for her assistance in sample analysis.

Literature Cited

(1) National Research Council. *Alternatives for Ground Water Cleanup*; National Academy Press: Washington, DC, 1994.
(2) Cohen, R. M.; Mercer, J. W. *DNAPL Site Evaluation*; C. K. Smoley: Boca Raton, FL, 1993.
(3) Pankow, J. F.; Cherry, J. A. *Dense Chlorinated Solvents and other DNAPLs in Groundwater*; Waterloo Press: Portland, OR, 1996.
(4) Jin, M.; Delshad, M.; Dwarakanath, V.; McKinney, D. C.; Pope, G. A.; Sepehrnoori, K.; Tilburg, C. E. *Water Resour. Res.* **1995**, *31*, 1201−1211.
(5) Wilson, R. D.; Mackay, D. M. *Ground Water* **1995**, *34* (2), 241−249.
(6) Nelson, N. T.; Brusseau, M. L. *Environ. Sci. Technol.* **1996**, *30*, 2859−2863.
(7) Cooke, C. E. U.S. Patent Number 3,590,923, 1971.
(8) Deans, H. A. U.S. Patent Number 3,623,842, 1971.
(9) Tang, J. S. *SPE Formation Evaluation 33*; 1995.
(10) Hunkeler, D.; Hoehn, E.; Hohener, P.; Zeyer, J. *Environ. Sci. Technol.* **1997**, *31*, 3180−3187.
(11) Annable, M. D.; Rao, P. S. C.; Hatfield, K.; Graham, W. D.; Wood, A. L.; Enfield, K. G. *J. Environ. Eng.* **1998**, 498−503.
(12) Young, C. M.; Jackson, R. E.; Jin, M.; Londergan, J. Y.; Mariner, P. E.; Pope, G. A.; Anderson, F. J.; Houk, T. *Ground Water Monit. Remed.* **1999**, *19*, 84−94.
(13) Brusseau, M. L.; Nelson, N. T.; Cain, R. B. In *Innovative Subsurface Remediation: Physical, Chemical, and Characterization Technologies*; Brusseau, M. L., Sabatini, D., Gierke, J., Annoble, M. D., Eds.; American Chemical Society, Washington, DC, 1999.
(14) Hayden, N. J.; Linnemeyer, H. C. In *Innovative Subsurface Remediation: Physical, Chemical, and Characterization Technologies*; Brusseau, M. L., Sabatini, D. A., Gierke, J. S., Annable, M. D., Eds.; American Chemical Society: Washington, DC, 1999.
(15) ASTM. Standard Test Method for Particle-Size Analysis of Soils. ASTM D 422-63. In *1993 Annual Book of ASTM Standards. Vol. 04. 08*; ASTM: Philadelphia, PA, 1993; pp 93−99.
(16) Klute, A.; Dirksen, C. Hydraulic conductivity and diffusivity: Laboratory Methods. In *Methods of soil analysis Part 1-Physical and mineralogical methods*; Soil Science Society of America: Madison, WI, 1986; pp 687−734.
(17) Lenhard, R. J. *J. Contam. Hydrol.* **1992**, *9*, 243−269.
(18) Oostrom, M.; Dane, J. H. *Calibration and Automation of a Dual-Energy Gamma System for Applications in Soil Science*; Agronomy and Soils Department Series 145; Alabama Agricultural Experimental Station: Auburn University, AL, 1990.
(19) Oostrom, M.; Dane, J. H.; Missildine, B. C.; Lenhard, R. *J. Soil Sci.* **1995**, *160*, 28−42.
(20) Brusseau, M. L. *Water Resour. Res.* **1992**, *28*, 33−45.
(21) Mualem, Y. *Water Resour. Res.* **1976**, *12*, 513−522.
(22) Lenhard, R. J.; Parker, J. C. *Water Resour. Res.* **1976**, *23*, 2197−2206.

Received for review January 8, 1999. Revised manuscript received July 15, 1999. Accepted September 1, 1999.

ES990022P